• Dobrica, E., Ishii, H., Bradley, J.P., Ohtaki, K., Brearley, A.J. and the Hayabusa2 Science Team (2023) Nonequilibrium spherulitic magnetite in the Ryugu samples. Geochimica Cosmochimica Acta 346, 65-75 10.1016/j.gca.2023.02.003

NONEQUILIBRIUM SPHERULITIC MAGNETITE IN THE RYUGU SAMPLES

- 2 Elena Dobrică¹, Hope A. Ishii¹, John P. Bradley¹, Kenta Ohtaki¹, Adrian J. Brearley², Takaaki
- 3 Noguchi³, Toru Matsumoto^{4,3}, Akira Miyake³, Yohei Igami³, Mitsutaka Haruta⁵, Hikaru Saito^{6,7},
- 4 Satoshi Hata^{8,9}, Yusuke Seto¹⁰, Masaaki Miyahara¹¹, Naotaka Tomioka¹², Hugues Leroux¹³,
- 5 Corentin Le Guillou¹³, Damien Jacob¹³, Francisco de la Peña¹³, Sylvain Laforet¹³, Maya
- 6 Marinova¹⁴, Falko Langenhorst¹⁵, Dennis Harries¹⁶, Pierre Beck¹⁷, Thi H. V. Phan¹⁷, Rolando
- 7 Rebois¹⁷, Neyda M. Abreu¹⁸, Jennifer Gray¹⁹, Thomas Zega²⁰, Pierre-M. Zanetta²⁰, Michelle S.
- 8 Thompson²¹, Rhonda Stroud²², Kate Burgess²², Brittany A. Cymes²³, John C. Bridges²⁴, Leon
- 9 Hicks²⁴, Martin R. Lee²⁵, Luke Daly^{25,26,27}, Phil A. Bland²⁸, Michael E. Zolensky²⁹, David R.
- 10 Frank¹³, James Martinez³⁰, Akira Tsuchiyama^{31,32,33}, Masahiro Yasutake³⁴, Junya Matsuno³¹,
- Shota Okumura³, Itaru Mitsukawa³, Kentaro Uesugi³⁴, Masayuki Uesugi³⁴, Akihisa Takeuchi³⁴,
- 12 Mingqi Sun^{32,33,35}, Satomi Enju³⁶, Aki Takigawa³⁷, Tatsuhiro Michikami³⁸, Tomoki Nakamura³⁹,
- 13 Megumi Matsumoto³⁹, Yusuke Nakauchi⁴⁰, Hisayoshi Yurimoto⁴¹, Ryuji Okazaki⁴², Hikaru
- 14 Yabuta¹¹, Hiroshi Naraoka⁴², Kanako Sakamoto⁴⁰, Shogo Tachibana⁴³, Toru Yada⁴⁰, Masahiro
- 15 Nishimura⁴⁰, Aiko Nakato⁴⁰, Akiko Miyazaki⁴⁴, Kasumi Yogata⁴⁰, Masanao Abe^{40,45}, Tatsuaki
- Okada^{40,45}, Tomohiro Usui^{40,45}, Makoto Yoshikawa^{40,45}, Takanao Saiki^{40,45}, Satoshi Tanaka^{40,45},
- 17 Fuyuto Terui⁴⁶, Satoru Nakazawa^{40,45}, Sei-ichiro Watanabe⁴⁷, Yuichi Tsuda^{40,45}
- 19 ¹Hawai'i Institute of Geophysics & Planetology, the University of Hawai'i at Mānoa, Honolulu,
- 20 HI 96822, USA (dobrica@hawaii.edu),
- ²Department of Earth and Planetary Sciences, University of New Mexico, Albuquerque, NM.
- ³Division of Earth and Planetary Sciences, Kyoto University; Kitashirakawaoiwake-cho, Sakyoku,
- 23 Kyoto 606-8502, Japan.
- ⁴The Hakubi Center for Advanced Research, Kyoto University; Kitashirakawaoiwake-cho,
- 25 Sakyoku, Kyoto 606-8502, Japan
- ⁵Institute for Chemical Research, Kyoto University; Gokasho, Uji, Kyoto 611-0011, Japan.
- ⁶Institute for Materials Chemistry and Engineering, Kyushu University, Fukuoka 816-8580, Japan.
- ⁷Pan-Omics Data-Driven Research Innovation Center, Kyushu University, Fukuoka 816-8580,
- 29 Japan.

18

- 30 ⁸Department of Advanced Materials Science, Kyushu University, Fukuoka 816-8580, Japan.
- 31 ⁹The Ultramicroscopy Research Center, Kyushu University, Fukuoka 819-0395, Japan.

- 32 ¹⁰Department of Geosciences, Osaka Metropolitan University; Sugimoto 3-3-138, Sumiyoshi-ku,
- 33 Osaka 558-8585, Japan.
- 34 ¹¹Earth and Planetary Systems Science Program, Hiroshima University; 1-3-1 Kagamiyama,
- 35 Higashi-Hiroshima City, Hiroshima, 739-8526, Japan.
- ¹²Kochi Institute for Core Sample Research, X-Star, JAMSTEC; 200 Monobe Otsu, Nankoku,
- 37 Kochi 783-8502, Japan.
- 38 ¹³Université de Lille, CNRS, INRAE; Centrale Lille, UMR 8207-UMET-Unité Matériaux et
- 39 Transformations, F-59000 Lille, France.
- 40 ¹⁴Université de Lille, CNRS, INRAE; Centrale Lille, Université Artois, FR 2638-IMEC-Institut
- 41 Michel-Eugène Chevreul, F-59000 Lille, France.
- 42 ¹⁵Institute of Geoscience, Friedrich Schiller University Jena; Carl-Zeiss-Promenade 10, D-07745
- 43 Jena, Germany.
- 44 ¹⁶Luxembourg Institute of Science and Technology, European Space Resources Innovation
- 45 Centre; Belvaux, Luxembourg.
- 46 ¹⁷Institut de Planétologie et d'Astrophysique de Grenoble (IPAG), Université Grenoble Alpes; CS
- 47 40700, 38058 Grenoble, cedex 09, France.
- 48 ¹⁸Langley Research Center, NASA; 1 Nasa Dr, Hampton, VA, USA.
- 49 ¹⁹Materials Characterization Lab, The Pennsylvania State University; Millennium Science
- 50 Complex, Pollock Road, University Park, PA USA.
- 51 ²⁰Lunar and Planetary Laboratory, Department of Planetary Sciences, University of Arizona; 1629
- 52 E. University Blvd., Tucson AZ 85721-0092, USA.
- 53 ²¹Department of Earth, Atmospheric and Planetary Sciences, Purdue University; 550 Stadium Mall
- Drive, West Lafayette, IN 47907-2051, USA.
- 55 ²²Materials Science and Technology Division, U.S. Naval Research Laboratory; Washington, DC
- 56 20375, USA.
- 57 ²³NRC Postdoctoral Research Associate, U.S. Naval Research Laboratory; Washington, DC
- 58 20375, USA.
- 59 ²⁴Space Park Leicester, University of Leicester, LE4 5SP, UK.
- 60 ²⁵School of Geographical and Earth Sciences, University of Glasgow; Gregory Building, Lilybank
- 61 Gardens, Glasgow G12 8QQ, UK.

- 62 ²⁶Australian Centre for Microscopy and Microanalysis, University of Sydney; Sydney, New South
- Wales, Australia.
- 64 ²⁷Department of Materials, University of Oxford; Oxford, UK.
- 65 ²⁸School of Earth and Planetary Sciences, Curtin University; GPO Box U1987, Perth, Western
- 66 Australia 6845, Australia.
- 67 ²⁹ARES, NASA, Johnson Space Center; 2101 NASA Parkway, Houston, Texas 77058, USA
- 68 ³⁰Jacobs Engineering; 1999 Bryan Street, Suite 1200, Dallas, Texas 75201, USA.
- 69 ³¹Research Organization of Science and Technology, Ritsumeikan University; 1-1-1 Nojihigashi,
- 70 Kusatsu, Shiga 525-8577, Japan.
- 71 ³²CAS Key Laboratory of Mineralogy and Metallogeny/Guangdong Provincial Key Laboratory of
- 72 Mineral Physics and Materials, Guangzhou Institute of Geochemistry, Chinese Academy of
- 73 Sciences (CAS); Guangzhou 510640, China.
- 74 33CAS Center for Excellence in Deep Earth Science; Guangzhou 510640, China.
- 75 ³⁴Japan Synchrotron Radiation Research Institute; 1-1-1 Kouto, Sayo-cho, Sayo-gun, Hyogo 679-
- 76 5198, Japan.
- 77 ³⁵University of Chinese Academy of Sciences; Beijing 100049, China.
- 78 ³⁶Department of Mathematics, Physics, and Earth Science, Ehime University; 2-5 Bunkyo-cho,
- 79 Matsuyama, Ehime 790-8577, Japan.
- 80 ³⁷Department of Earth and Planetary Science, University of Tokyo; 7-3-1 Hongo, Bunkyo-ku,
- 81 Tokyo 113-0033, Japan.
- 82 ³⁸Faculty of Engineering, Kindai University; Hiroshima Campus, 1 Takaya Umenobe, Higashi-
- 83 Hiroshima, Hiroshima 739-2116, Japan.
- 84 ³⁹Department of Earth Science, Graduate School of Science, Tohoku University; 6-3 Aoba,
- 85 Aramaki, Aoba-ku, Sendai 980-8578, Japan.
- 86 ⁴⁰Institute of Space and Astronautical Science, Japan Aerospace Exploration Agency; 3-1-1
- 87 Yoshinodai, Chuo-ku, Sagamihara, Kanagawa 252-5210, Japan.
- 88 ⁴¹Department of Earth and Planetary Sciences, Hokkaido University; Kita-10 Nishi-8, Kita-ku,
- 89 Sapporo 060-0810, Japan.
- 90 ⁴²Department of Earth and Planetary Sciences, Kyushu University; 744 Motooka, Nishi-ku,
- 91 Fukuoka 819-0395, Japan.

- 92 ⁴³UTokyo Organization for Planetary and Space Science, University of Tokyo; 7-3-1 Hongo,
- 93 Bunkyo-ku, Tokyo 113-0033, Japan.
- 94 ⁴⁴Marine Works Japan Ltd.; 3-54-1, Oppamahigashi-cho, Yokosuka 237-0063, Japan.
- 95 ⁴⁵The Graduate University for Advanced Studies, SOKENDAI; Hayama 240-0193, Japan.
- 96 ⁴⁶Department of Mechanical Engineering, Kanagawa Institute of Technology; Atsugi 243-0292,
- 97 Japan.
- 98 ⁴⁷Department of Earth and Environmental Sciences, Nagoya University; Furo-cho, Chikusa-ku,
- 99 Nagoya 464-8601, Japan.

Abstract

We have investigated two particles collected during each of two touchdowns of the Hayausa2 spacecraft at the surface of the C-type asteroid 162173 Ryugu using various electron microscope techniques. Our detailed transmission electron microscopy study shows the presence of magnetite with various morphologies coexisting in close proximity. This is characteristic of CI chondritelike materials and consistent with the mineral assemblages and compositions in the Ryugu parent body. We describe the microstructural characteristics of magnetite with different morphologies, which could have resulted from the chemical conditions (growth vs. diffusion rate) during their formation. Furthermore, we describe the presence of magnetites with a spherulitic structure composed of individual radiating fibers and that are characterized by pervasive, homogeneously distributed euhedral to subhedral pores that have been described in previous chondrite studies. This particular spherulitic structure is consistent with crystallization under nonequilibrium conditions. Additionally, the presence of a high density of defects within the magnetite fibers, the high surface/volume ratio of this morphology, and the presence of amorphous materials in several pores and at the edges of the acicular fibers further support their formation under nonequilibrium conditions. We suggest that the growth processes that lead to this structure were imposed by the reach of the solution of a supersaturated state, resulting in the adjustment to a lower free energy condition.

Introduction

Samples returned from the carbonaceous asteroid 162173 Ryugu by the Japan Aerospace Exploration Agency (JAXA)'s Hayabusa2 mission allow us to investigate primitive materials from a known target and their evolution (Yada et al., 2022; Nakamura et al., 2022; Yokoyama et al., 2022). Recent studies have shown that the Ryugu samples are composed of minerals similar to those of CI (Ivuna-like) carbonaceous chondrites indicating that the parent planetesimal from which Ryugu was derived experienced severe aqueous alteration (Yada et al., 2021; Ito et al., 2022; Nakamura et al. 2022; Noguchi et al., 2022; Okazaki et al., 2022; Yokoyama et al., 2022). The present study focuses on magnetite (Fe³⁺(Fe²⁺Fe³⁺)₂O₄), which is one of the main minerals in the Ryugu samples (Nakamura et al., 2022) that was formed during these aqueous alteration events. The modal abundances of magnetite are similar in samples between the first (chamber A, 3.4 ± 1.6 vol%) and second touchdowns (chamber C, 3.7 ± 1.7 vol%; Nakamura et al., 2022). However, the

magnetite abundance in the Ryugu asteroid is lower than in the CI chondrites (4.3 vol\%, Alfing et al., 2019). Magnetite has been described in all Solar System materials, including chondritic meteorites (comprising carbonaceous chondrites (CCs) and ordinary chondrites (OCs)), Antarctic micrometeorites (AMMs), interplanetary dust particles (IDPs), and samples returned from the Moon, comet 81P/Wild 2, and asteroid Itokawa (Jedwab, 1967; Kerridge et al., 1979; Schramm et al., 1989; Rowe et al., 1994; Genge et al., 1997; Hua and Buseck, 1998; Noguchi et al., 2002; Brearley, 2006; Zolensky et al., 2008; Stodolna et al., 2012; Blinova et al., 2014; Doyle et al., 2015; Joy et al., 2015; Hicks et al., 2017; Noguchi et al., 2017; Jilly-Rehak et al., 2018; Dobrică et al., 2019; Burgess and Stroud, 2021; Nakamura et al., 2022). However, magnetite only displays a unique variety of morphologies in CI chondrites and the ungrouped carbonaceous chondrite Tagish Lake, similar to the Ryugu samples (Jedwab, 1967; Kerridge et al., 1979; Hua and Buseck, 1998; Blinova et al., 2014). Three major magnetite types have been identified: framboidal, spherules, and plaquette (Hua and Buseck, 1998). These complex morphologies were previously described in numerous studies starting in the 1960s (Ramdohr, 1963; Jedwab, 1965; Jedwab, 1967; Hua and Buseck, 1998; Chan et al. 2016). However, the conditions that constrain the formation of magnetite to each of these particular morphologies remain unknown. Better understanding of their formation mechanisms is essential to interpret if these different morphologies provide information about the evolution history of the aqueous alteration processes on the Ryugu asteroid.

Magnetite is known to form in igneous, metamorphic, and sedimentary settings and through different reactions such as gas and liquid interactions on Earth, in the solar nebula, and on small Solar System parent bodies (Kerridge et al., 1979; Mittlefehldt et al., 1998; McSween and Treiman, 1998; Krot et al., 1997; Keller, 1998; Klein 2005; Chaumard et al., 2009; Hicks et al., 2017; Barth et al., 2018; Izawa et al., 2019). As a consequence, it is a useful mineral for studying a variety of processes such as variation in oxygen fugacity, paleomagnetism, water-rock interactions, and biogenic activity (McKay et al., 2003; Izawa et al., 2019; Sato et al. 2022). In chondrites, petrographic evidence suggests that magnetite is often formed during post-accretional aqueous alteration processes (Krot et al. 1997; Hua and Buseck, 1998; Brearley, 2006; Alfing et al., 2019). Kerridge et al. (1979) first proposed that magnetite in CI chondrites formed on the meteorite parent body from an aqueous gel-like phase containing colloidal crystals. Recent studies suggest that the formation of colloidal crystals implies several restrictions on the growth conditions, such as (1) supersaturation of the aqueous fluid; (2) confinement of the aqueous fluid in small voids, in which

colloidal crystallization takes place; and (3) nucleation occurring in a short period of time, with no further nucleation during subsequent growth (Nozawa et al., 2011; Kimura et al., 2013). The last restriction points to a sudden change in the conditions in the parent body, for instance, a change in temperature, pressure, or fluid composition, which rapidly alters the supersaturation or the temperature of the solution (Nozawa et al., 2011). Therefore, the objective of this study is to understand the formation mechanisms of magnetite and especially those with a spherulitic structure (a.k.a. spherulitic magnetite). We investigated several particles collected during both landing operations (from chamber A and chamber C) of the Hayabusa2 mission. The goal of this study is to assess the evolution of the aqueous alteration processes on carbonaceous (C-type) asteroids.

Samples and Methods

Multiple Ryugu particles returned by the Hayabusa2 spacecraft and collected during each of the two touchdowns (collected in chambers A and C, respectively, Tachibana et al., 2022) were analyzed in this study (Figs. 1-6). Four focused ion beam (FIB) sections were prepared and analyzed at Kyoto University, University of Hawai'i at Mānoa, University of New Mexico, and University of Lille using different electron microscopes (scanning and transmission electron microscopes). Additionally, we analyzed one stub (C0105-039) with multiple grains collected during the second landing operation (chamber C). The stub was characterized by scanning electron microscopy (SEM) using backscattered electron imaging on a Helios 660 dual-beam focused ion beam SEM (FIB-SEM) instrument at the Advanced Electron Microscopy Center (AEMC) at the University of Hawai'i at Mānoa.

Each electron transparent section was prepared by the conventional *in situ* FIB technique: a platinum protective layer was deposited on top of the region of interest, first by electron beam deposition and then by ion beam deposition, to avoid gallium primary ion beam damage during the FIB sample preparation. The section was transferred to Cu TEM half grid with a micromanipulator. The final ion milling of the 2 µm thick section to electron transparency was carried out with the sample attached to the TEM grid. The final thinning stages were performed at 2 kV with a current of 72 pA.

All FIB sections were studied using a variety of transmission electron microscopy (TEM) techniques, including scanning transmission electron microscopy (STEM) imaging, nanobeam

diffraction (NBD), and energy-dispersive X-ray spectroscopy (EDS). The imaging and analyses were carried out at 200 kV and 300 kV using the Titan G2 analytical (S)TEM at the AEMC, the TitanX at the Molecular Foundry, Lawrence Berkeley National Laboratory, the JEOL NEOARM 200CF aberration-corrected STEM/TEM instrument at the Nanomaterial Characterization Facility at the University of New Mexico (UNM), the JEOL JEM 2100F at the Kyoto University, and Titan Themis 300 S/TEM at the University of Lille. Nanobeam diffraction was obtained in the STEM mode condition and carried out using a collection semi-angle of 0.3 mrad. Mineral phases were identified by their elemental compositions, in addition to subsequent electron diffraction. Additional EDS hyperspectral maps of the sample A104-01300103 were collected at the University of Lille. For STEM-EDX elemental analysis the probe size has been about 2 nm, semiconvergence angle 10 mrad and probe current of about 300 pA. The STEM-EDX mapping has been performed with a dwell time of 5 µm/px with continuous scanning over a series of up to 900 frames during a total time of 10-15 min per acquisition. The elemental maps represent a sum of the total number of frames. Compositions were normalized to 100% of detectable elements. The EDS detection limit for major elements during the TEM measurements is estimated to be <0.5 at%. Oxygen abundances should be viewed with caution (calculated oxide) because oxygen K Xrays are subject to variable amounts of self-absorption by the sample. The EDS measurements of the sample from chamber C were acquired using the JEOL NEOARM 200CF at UNM, which is equipped with dual JEOL 100 mm² EDS detectors controlled using Oxford Instruments AZtec software.

213

214

215

216

217

218

219

220

221

222

223

193

194

195

196

197

198

199

200

201

202

203

204

205

206

207

208

209

210

211

212

Results

The SEM images of several Ryugu particles collected during the second landing operation (in chamber C) show the presence of magnetite grains with a variety of different morphologies, including framboids (Fig. 1a), plaquettes (Fig. 1b), and spherules (Fig. 1c-f). The framboidal magnetites are generally found as aggregates up to 8 μm in length, composed of euhedral magnetite crystals. However, some of the individual crystals embedded in the fine-grained matrix of phyllosilicates are faceted (e.g., single dodecahedron, Fig. 1c). The largest dodecahedron observed is 4 μm in diameter (Fig. 1c). Magnetite plaquette aggregates are composed of magnetite discs with a constant thickness of ~0.15 μm. Magnetite spherules are common in the Ryugu samples and are characterized by either (1) a spherulitic structure defined by radiating fibers of magnetite

(a.k.a. spherulitic magnetite, Fig. 1e-f) or (2) they are texturally featureless (a.k.a. magnetite spherules, see Fig. 1 and Yokoyama et al., 2022). The magnetites with a spherulitic structure are easy to identify in backscattered electron (BSE) images (Fig. 1e); however, their fibrous surface structure is difficult to distinguish in the secondary electron (SE) image (Fig. 1f) because some regions are covered with thin layers of phyllosilicates. Generally, the magnetite spherules that are texturally featureless are similar in size (~10-15 μm in diameter, Yokoyama et al., 2022) to those with a spherulitic structure (~13 µm in diameter, Fig. 1e-f). However, several small magnetite spherules (~1 µm in diameter, Fig. 1) that are texturally featureless were identified in the FIB sections analyzed (Figs. 3a, 4, see further details below). In this study, we distinguish between magnetite spherules and framboidal magnetite which differ by their size and dispersion. Framboidal magnetites are generally characterized by densely packed aggregates of framboid crystal with a constant sizes distribution (avg. 0.5 µm); however, magnetite spherules are anhedral to subhedral and sparsely distributed with crystals that have variable sizes (0.35-1.2 µm, Figs. 1a, 3a, 4). Figure 1a shows the association of framboidal and texturally featureless magnetite spherules. All magnetite grains are embedded in a fine-grained material composed of phyllosilicates, euhedral sulfides, and carbonates. Detailed TEM observations confirm that magnetite with two different morphologies is present in the four FIB sections analyzed in this study: (1) framboidal (Fig. 2a – A0104-00200201) and (2) spherules either with a spherulitic structure (Fig. 2 – A0104-00200201, Fig. 3 – C0105-039024, Fig. 5 – A0104-00100401, and Fig. 6 – A104-01300103), or texturally featureless spherules (Fig. 3a – C0105-039024 and Fig. 4 – A104-01300103). No magnetite plaquettes were present in the TEM samples analyzed in this study. The framboidal aggregate observed is $\sim 3 \times 5.3$ µm in size and is composed of euhedral magnetite crystals with a constant size (~500 nm in diameter). A few texturally featureless magnetite spherules are present in the FIB sections (Figs. 3-4). These anhedral spherules vary in size from 0.6 µm to 1.2 µm in diameter (Figs. 3-4). However, in this study, we focus on magnetite spherules that show a spherulitic structure identified in the FIB sections. Four spherulitic magnetites were analyzed in this study. They vary in size from ~2.9 µm in length and \sim 2 µm wide (sample A0104-00200201, Fig. 2) to \sim 13-16 µm in size (sample C0105-039024, Fig. 3). Most of the spherulite analyzed have a regular, nearly spherical external shape with the exception of one spherulitic magnetite from sample A0104-00100401, which is irregular in shape (Fig. 5). In this heterogeneous spherulite the fibers vary in length from 0.9 µm to 2.3 µm

224

225

226

227

228

229

230

231

232

233

234

235

236

237

238

239

240

241

242

243

244

245

246

247

248

249

250

251

252

253

(see further details below). All spherulitic magnetites, except the one irregular in shape (A0104-00100401, Fig. 5) are characterized by three main features. First, their structure is composed of individual radiating fibers, which vary in length from 0.8 µm to 8 µm for the three regular shaped spherulites analyzed in this study (Figs. 2-3, 5-6). The widths of the fibers vary in size from 70 nm to 140 nm. These spherulitic magnetites are essentially single crystals. Therefore, all fibers have the same crystallographic orientation even if they are not in contact with each other, as indicated in two of the multiple diffraction patterns measured in these grains that are shown in Figure 3b-d. However, some domains may have slight misorientations. The surface of the spherulitic magnetites shows euhedral laths of the radiating fibers, with laths up to ~50 nm wide. The fibers radiate from a spherical pore (~130 nm in diameter) located off-center in sample C0105-039024 (Figs. 3a and 3g). However, in two of the spherulitic magnetites analyzed (A0104-0020020 – Fig. 5 and A104-01300103 – Fig. 6), no central pore was identified in the region where the magnetite fibers start radiating. This could be because the FIB section did not intersect the central pore. Second, numerous nanometric euhedral to subhedral pores were identified mainly decorating the boundaries between the fibers. These pervasive pores were identified in all spherulitic magnetites (Figs. 2-3), except the irregular shaped spherulitic magnetite. Their sizes vary from a few nanometers up to ~2.2 μm in length, and they are homogeneously distributed in both spherulite magnetites. The pores are located mainly at the boundaries between the fibers; however, the thickness of the FIB sections is larger than the size of the pores, so it is difficult to exclude their presence inside the magnetite fibers. In sample C0105-039024, most euhedral pores are elongated parallel to the radiating fibers (Fig. 3h). The pores are absent in the framboidal cluster (Fig. 2) that coexist in close proximity to the spherulitic magnetite. However, the several magnetite spherules contain anhedral to subhedral pores up to a few tens of nanometer in diameter (Fig. 4, sample A104-01300103); however, no pores were observed in the magnetite spherules from sample A0104-00200201 (Fig. 2a). Third, diffraction contrast STEM images (Fig. 3e-f) show the occurrence of pervasive dislocations in the magnetite fibers (Fig. 3e-f). Most of these features are visible only in the STEM micrographs taken using a convergent angle 2α of the electron beam of 0.3 mrad that provides better contrast, especially in deformed crystals (Alloyeau et al., 2008; Zhu et al., 2018).

255

256

257

258

259

260

261

262

263

264

265

266

267

268

269

270

271

272

273

274

275

276

277

278

279

280

281

282

283

284

285

Several differences are observed between the irregular shaped spherulitic magnetite and those with a regular, spherical, shape. First, no pores were identified in this magnetite. Second, the

irregular shaped spherulitic magnetite consists of multiple crystal domains (~100 nm in diameter), some of which show 3-fold periodicity along one of the <111> directions (Fig. 5). The neighboring crystals in the aggregate have epitaxial relationships.

No clear evidence of space weathering was observed in the magnetite crystals identified in these FIB sections. However, a recent study shows that framboidal and spherulitic magnetite surfaces could be modified by solar wind implantation and micrometeorite impacts (Matsumoto et al. 2022). The compositions of these magnetites were measured by EDS/TEM and no elements other than oxygen and iron were identified. However, one spherulitic magnetite (sample A104-01300103, Fig. 6) contains Si- and Mg-rich amorphous materials at the edges of the acicular fibers (Fig. 6d-e). Furthermore, we identified amorphous Si-rich materials in several pores (Fig. 6a-c). Table 1 shows the chemical composition of these nonstoichiometric amorphous materials.

Additionally, associated with magnetite in the FIB sections analyzed, we identified sulfides and organic nanoglobules (430 x 630 nm in size) that are embedded in a groundmass consisting of coarse-grained phyllosilicates (up to ~150 nm in length), with basal spacings of 1 nm.

Discussion

Ryugu samples have been shown to resemble a CI chondrite that exhibit some notable differences from CI meteorites (Yada et al., 2021; Nakamura et al. 2022; Yokoyama et al., 2022). One of the major similarities in Ryugu asteroid to CI chondrites is the presence of magnetites with different morphologies. Magnetite with a variety of morphologies has been studied for almost sixty years in one of the rarest groups of meteorites, the CI chondrites (only 9 meteorites belong to this group), and more recently in the unique, ungrouped Tagish Lake meteorite (Jedwab, 1967; Kerridge et al., 1979; Hua and Buseck, 1998; Brearley, 2006; Kimura et al. 2013). Our TEM observations further expand on the implications of magnetite formation in the Ryugu samples that show some difference to known CI chondrites (Yada et al., 2022; Nakamura et al., 2022; Yokoyama et al., 2022). The observations presented in this study show the presence of magnetite with different morphologies coexisting in close proximity. Further discussion focuses on magnetite with a spherulitic structure that exhibits unique porosity that has not been described in previous studies. Previous studies have suggested that all spherical magnetites in CI meteorites possess a spherulitic structure and that those without a structure may have lost their structure during polishing (Kerridge et al., 1979). However, our TEM observations show that both structures of

spherules (either a spherulitic structure or texturally featureless) coexist in the Ryugu samples and that they are not a product of sample preparation.

Formation of spherulitic magnetite

Spherulites are common in terrestrial and extraterrestrial materials (Kerridge et al., 1979; Gránásy et al., 2005; Shtukenberg et al., 2012; Zheng et al., 2019). They have been identified in a wide range of materials such as metals, alloys, polymers, oxides, liquid crystals, and various biological molecules. Spherulites are generally defined as two- or three-dimensional branched solids with nearly spherical external shapes but notable internal textures. In contrast to dendritic structures with fractal branches, spherulites have more densely packed branches (Zheng et al., 2019). Shtukenberg et al.'s (2012) review of spherulites offers a detailed description of their formation and growth conditions, indicating that any substance (melt, amorphous solids, solutions, and gels) can be made to adopt a spherulitic morphology under some conditions. However, so far, there is no generally accepted theory that constrains spherulite crystallization mechanisms. The most important prerequisite for spherulitic growth is high crystallization driving forces, typical from a supersaturated or supercooled solution (Shtukenberg et al., 2012). Recently, the formation of iron oxide spherulites was directly observed in real-time, at a subnanometer resolution in a liquid cell using transmission electron microscopy (Zheng et al., 2019). In this experiment, the growth was initiated rapidly by electron beam irradiation of the solution. Other rapid, dynamic processes, such as quenching, spontaneous precipitation, and agitation processes are often described as the principal mechanisms used to explain the formation of spherulites (Grassmann et al., 2004; Gránásy et al., 2005; Prus et al., 2021; Cui et al., 2022).

Furthermore, spherulites are ubiquitous in solids formed under nonequilibrium conditions (Magill, 2001; Gránásy et al., 2005; Siódmiak and Gadomski, 2022). Systems that are in equilibrium tend to grow crystals with simple morphologies unless they are forced out of equilibrium by imposing a change in the environmental conditions (Magill, 2001). Therefore, crystals can form complex spatial patterns in response to a disturbance from equilibrium that might induced kinetically driven growth to lower the free energy of the system. Though there are other factors that can influence the morphologies of crystals. For example, the presence of organic compounds can play a major role influencing growth of crystals by inhibiting growth on some crystal surfaces and favoring one morphology over another (Xu et al., 2014; Nakamura et al.,

2022). Similarly, it is also possible that due to polarity certain anions or cations in solution can change the growth mechanism and change the morphology (Wark et al. 2008).

348

349

350

351

352

353

354

355

356

357

358

359

360

361

362

363

364

365

366

367

368

369

370

371

372

373

374

375

376

377

378

In chondrites, multiple petrographic studies and thermodynamic models have suggested that aqueous precipitation of minerals occurred during local and temporal solution-solid equilibration (Zolensky et al., 1989; Bourcier and Zolensky, 1992; Rosenberg et al., 2001; Schulte and Shock, 2004; McAlister and Kettler, 2008; Zolotov, 2012; Nakamura et al., 2022). However, evidence for nonequilibrium conditions, such as the presence of porous, amorphous, and spherulitic materials, and high surface/volume ratio textures, are observed in primitive meteorites and in hydrothermal experiments performed at conditions informed by our current state of knowledge of asteroidal alteration (Gránásy et al., 2005; Dobrică et al., 2022). For example, pores have been described previously in other materials that form under nonequilibrium conditions, such as euhedral, FeOrich olivines, which are similar to the ones described in CK and CV chondrites (Brearley, 1999, 2009; Dobrică et al., 2022). However, it remains unclear why several magnetite spherules contain pores even if they do not show other characteristics for their formation during nonequilibrium processes (Fig. 4). Intra-crystalline porosity is still a poorly understood phenomenon, but is always attributed to the deposition and entrapment of a macromolecular phase at crystal surfaces (Rizzato et al., 2016). Furthermore, defects underlie spherulitic growth (Shtukenberg et al., 2012). It has been shown that the dislocation density increases as the spherulitic crystal grows (Shtukenberg et al., 2012). Additionally, pores are an important source of "defects" when crystallizing spherulites impinge (Magill, 2001). During crystallization, numerous small pores may accumulate at the impinging spherulite boundaries (Magill, 2001). The presence of amorphous, nonstoichiometric materials inside the pores and at the edges of the spherulitic fibers further supports the formation of spherulitic magnetite through nonequilibrium reactions. The amorphous materials probably formed from the remaining fluid or gel-like material, which probably contained, in addition to Fe hydroxide, minor amounts of Si and Mg (Fig. 6). Previous studies of carbonaceous chondrite matrices have suggested the formation of a gel-like phase, as a result of the modification during hydration processes of precursor anhydrous amorphous silicates at low temperatures, at near neutral pH and relatively oxidizing conditions (Zolensky et al., 1989; Chizmadia and Brearley, 2008; McCollom et al., 2013; Le Guillou and Brearley, 2014; Le Guillou et al., 2015). Therefore, since all spherulitic magnetites identified in the Ryugu samples are characterized by a high surface/volume ratio due to the individual fibers at the surface of each magnetite grain, unique

porosity, amorphous Si- and Mg-rich materials, and a high density of defects, we suggest that they were formed under nonequilibrium conditions (Kerridge et al., 1979; Magill, 2001; Gránásy et al., 2005; Smith et al., 2001; Shtukenberg et al., 2012; Siódmiak and Gadomski, 2022; Dobrică et al., 2022).

379

380

381

382

383

384

385

386

387

388

389

390

391

392

393

394

395

396

397

398

399

400

401

402

403

404

405

406

407

408

409

Additionally, previous studies of spherulites in meteorites suggested that this particular structure requires crystallization from a colloidal Fe hydroxide gel-like material (Kerridge et al., 1979). Studies of terrestrial spherulite show that a viscous medium (i.e., gel) is not always necessary for spherulitic growth; however, impurities encourage spherulite formation (Shtukenberg et al., 2012). The conditions necessary for the spherulite precipitation must maintain the growth rates (G) of the crystal itself higher than diffusion rates (D, G >> D, Lofgren, 1974; Kerridge et al., 1979). Previous studies showed that in a gel-like material compared with a solution system, convection is eliminated, and thus the mass transport is merely diffusive (Velásquez-González et al., 2019). Any changes related to variation in D/G ratio could generate crystals with different morphologies (Lofgren, 1974). Therefore, the presence of magnetite in the returned samples with varying crystal morphologies, including the irregular shaped spherulitic magnetite suggests a variable range of crystal growth and diffusion rates in the Ryugu parent body. Furthermore, it has been suggested that gels could strongly inhibits the crystal nucleation with a preferential formation of fewer larger crystals rather than many smaller ones (Talla and Wagner, 2022). Since few nuclei appear in a gel, this confirms that nucleation should occur at higher supersaturation in gel than in solution systems (Lefaucheux et al., 1982). The extent of nucleation suppression can vary by using different gel concentrations, with a high concentrated gel that generally leads to the formation of rounded individuals or radial spherulites (Talla and Wagner, 2022). Therefore, in addition to the crystal growth and diffusion rates, the gel concentration could have played an important role in the formation of magnetite with variable crystal morphologies.

Petrographic observations suggested that magnetites with a spherulitic morphology are one of the first minerals to crystallize from an aqueous fluid on the Ryugu parent body (Tsuchiyama et al., 2022). More precisely, the crystallization sequence of magnetite as a function of their morphologies is suggested to be: spherulitic – plaquette/framboidal – equant/elongated (Tsuchiyama et al., 2022). This previous study indicated that the conditions during magnetite precipitation changed from high to low supersaturations (Tsuchiyama et al., 2022), which supports our observations that the first magnetites that formed, the spherulitic crystals, precipitated from a

highly supersaturated fluid that evolved in the degree of saturation. Our TEM study further expands on these results suggesting that at the beginning of the crystallization sequence, when the spherulitic magnetite formed, the fluid could have been under nonequilibrium conditions. These processes lead to polycrystalline growth structures imposed by the reach of the solution of a supersaturated state where nucleation is able to occur, resulting in the adjustment to a lower free energy condition. Furthermore, as the previous petrographic observations suggested (Tsuchiyama et al., 2022), and the presence of numerous fragile, euhedral laths at the surfaces of these spherulitic magnetites, suggest that these crystals precipitated first in an unrestricted, high porous material.

Implications for the presence of spherulitic magnetite in the Ryugu samples

Magnetite is a particularly valuable tracer of a wide variety of processes. Three important implications arise from the study of spherulitic magnetite. First, our study shows evidence of magnetite formation under nonequilibrium condition suggesting a delicate balance between thermodynamics and kinetics, which govern the complicated dynamics of multiple episodes crystallization. These results are in agreement with previous studies, which indicated that CI chondrites were processed by multiple episodes of aqueous alteration under varying physical and chemical conditions (Endreß and Bischoff, 1996).

Second, these crystals could potentially offer a unique opportunity to study the early aqueous fluids that circulated through the Ryugu parent body. No materials were identified in the unique pores identified in the spherulitic magnetite due to the sample preparation technique applied in this study; however, it is possible that these pores contain fluid inclusions prior to the FIB sample preparation. Some of the pores have perfect negative crystal shapes, i.e., the pores are polyhedral with their facets corresponding to rational planes of the host crystal (Cesare et al., 2021). Primary fluid inclusions are thought to be trapped only very rarely with negative crystal shapes (Roedder, 1984). However, if some fibers grow faster than others, the surfaces of the crystal can become rough, having many angular reentrant features, and later growth covering these reentrants produces negative crystal cavities (Roedder, 1984). Primary (trapped during growth) and secondary (trapped at a later time along a healed fracture) fluid inclusions were first reported in Monahans and Zag halite and present proof that aqueous fluid inclusions exist in some extraterrestrial samples, and have led to a renewed search in other extraterrestrial samples (Zolensky et al., 1999; Zolensky et al., 2017; Tsuchiyama et al. 2021; Zolensky et al., 2022). Recently, Nakamura et al. (2022) and

Zolensky et al. (2022) identified fluid inclusions in pyrrhotite crystals in the Ryugu samples collected during the second touchdown (chambers C). These ancient fluids were trapped in the during the crystal growth and provide information on the water-rock interaction that took place on the Ryugu parent body. The chemical composition of the fluid inclusions identified in pyrrhotite from the Ryugu samples show the presence of a saline aqueous solution containing H₂O, CO₂, sulfur species, and nitrogen- and chondrite-bearing organic compounds (Nakamura et al., 2022; Zolensky et al., 2022). According to the crystallization sequence of the major secondary phases identified in the Ryugu samples, pyrrhotite crystals formed after the formation of magnetite, especially those with a spherulitic structure (Tsuchiyama et al., 2022). Therefore, the presence of any fluid inclusion in these spherulitic magnetites could provide a unique opportunity (1) to measure the chemical composition of the primary aqueous fluids on the Ryugu asteroid and (2) to understand the evolution of fluid chemistry during multistage events.

A third important implication that arises from the occurrence of spherulitic magnetite under nonequilibrium conditions is that a careful selection of the magnetite crystals is necessary for the use of the oxygen isotope fractionation between carbonates and magnetite to extract the temperature at which these minerals coprecipitated (Zheng, 2011; Jilly-Rehak et al., 2018; Dobrică et al., 2019; Yokoyama et al., 2022). Since multiple generations of magnetite were identified in the Ryugu samples, the question is what type of magnetite forms in equilibrium with the carbonates, especially since dolomite and breunnerite formed after the formation of pentlandite, pyrrhotite, and apatite according to the crystallization sequence (Tsuchiyama et al., 2022). We suggest avoiding spherulitic magnetite for these measurements since the necessary assumption of equilibrium between minerals is not supported by our observations indicating rapid magnetite growth.

Summary

Our TEM observations provide new insights into the complex formation of magnetite in the asteroid Ryugu. We describe the microstructural differences between magnetite with different morphologies, which could have resulted from the chemical conditions (growth vs. diffusion rate) that existed during their formation. Furthermore, we show for the first time that magnetites with a spherulitic structure are characterized by the presence of a unique porosity. Multiple characteristics such as (1) structure, (2) porosity, (3) high density of defects within the magnetite fibers, (4)

amorphous materials, and (5) the high surface/volume ratio of this structure indicate that they form through nonequilibrium processes. These processes lead to polycrystalline growth structures imposed by the reach of the fluid solution of a supersaturated state where nucleation is able to occur, resulting in the adjustment to a lower free energy condition. Therefore, their formation could have important implications in our fundamental understanding of the evolution of fluids on the Ryugu parent body.

Acknowledgments: We would like to thank Dr. C.M.O'D. Alexander for helpful comments and discussions. The Hayabusa2 project has been developed and led by JAXA in collaboration with Deutsches Zentrum für Luft- und Raumfahrt (DLR) and Centre national d'études spatiales (CNES), and supported by NASA and Australian Space Agency (ASA). We thank all of the members of the Hayabusa2 project for their technical and scientific contributions. Matsumoto T. is supported by JSPS grants (No. 21K13981 and 21H05431). AJB is supported by NASA Emerging Worlds grant 80NSSC18K0731 and the JEOL NEOARM at the University of New Mexico by NSF MRI grant 1828731. Analytical work at the University of Hawai'i at Mānoa was supported by the Hawai'i Institute of Geophysics & Planetology. Work at the Molecular Foundry was supported by the Office of Science, Basic Energy Sciences, of the U.S. Department of Energy under Contract No. DE-AC02-05CH11231.

- 490 References
- Alfing, J., Patzek, M., Bischoff, A., 2019. Modal abundances of coarse-grained (>5 μm)
- components within CI-chondrites and their individual clasts Mixing of various lithologies
- on the CI parent body(ies). Geochemistry, 79, 125532.
- 494 Alloyeau, D, Ricolleau, C., Oikawa, T., Langlois, C., Le Bouar, Y., Loiseau, A. 2008. STEM
- 495 nanodiffraction technique for structural analysis of CoPt nanoparticles. Ultramicroscopy,
- 496 108, 656-662.
- Barth, M. I. F., Harries, D., Langenhorst, F., Hoppe, P., 2018. Sulfide-oxide assemblages in
- Acfer 094—Clues to nebular metal–gas interactions. Meteorit. Planet. Sci. 53, 187-203.
- Blinova, A.I., Zega, T. J., Herd, C. D. K., Stroud, R. M., 2014. Testing variations within the
- Tagish Lake meteorite I: Mineralogy and petrology of pristine samples. Meteorit. Planet. Sci.
- 501 49, 473-502.
- Bourcier, W. L., Zolensky, M. E., 1992. Computer modeling of aqueous alteration on
- 503 carbonaceous chondrite parent bodies. Lunar Planet. Sci. Conf. 23. abstr. 143-144.
- Brearley, A. J., 1999. Origin of graphitic carbon and pentlandite in matrix olivines in the
- Allende meteorite. Science 285, 1380-1382.
- Brearley, A. J., 2006. The action of water. In Meteorites and the early solar system II, edited by
- Lauretta D. S. and McSween H. Y. Jr. Tucson, Arizona: University of Arizona Press. pp.
- 508 584-624.
- Brearley, A. J., 2009. Matrix olivines in the metamorphosed CK chondrite NWA 1628: Possible
- affinities to olivines in the matrices of oxidized CV3 chondrites and dark inclusions. Lunar
- 511 Planet. Sci. Conf. 40. abstr. #1791.
- Burgess, K. D. Stroud, R. M., 2021. Exogenous copper sulfide in returned asteroid Itokawa
- regolith grains are likely relicts of prior impacting body. Comm. Earth Env. 2, 115.
- Cesare, B., Parisatto, M., Mancini L., Peruzzo, L., Franceschi, M., Tacchetto, T., Reddy, S.,
- Spiess, R., Nestola, F., Marone, F., 2021. Mineral inclusions are not immutable: Evidence of
- post-entrapment thermally-induced shape change of quartz in garnet. Earth Planet. Sci. Lett.
- 517 555, 116708.
- Chan, Q., Zolensky, M. E., Martinez, J., Tsuchiyama, A., Miyake, A. 2016. Magnetite
- 519 plaquettes are naturally asymmetric materials in meteorites. American Mineralogist 101,
- 520 2041–2050.

- Chaumard, N., Devouard, B., Zanda, B., Ferriere, L., 2009. The link between CV and CK
- carbonaceous chondrites based on parent body processes. In: 72nd Annual Meeting of the
- 523 Meteoritical Society, abstr. #5206.
- 524 Chizmadia, L. J., Brearley, A. J., 2008. Mineralogy, aqueous alteration, and primitive textural
- characteristics of fine-grained rims in the Y-791198 CM2 carbonaceous chondrite: TEM
- observations and comparison to ALHA81002. Geochim. Cosmochim. Acta 72, 602–625.
- 527 Cui, P., Yang, W., Jia, L., Zhou, L., Zhang, M., Bao, Y., Xie, C., Hou, B., Yin Q., 2022.
- 528 Spherulitic growth strategy for agitation-induced formation of spherical amoxicillin sodium
- 529 products. Ind. Eng. Chem. Res. 61, 9821-9832.
- Dobrică, E., Ogliore, R.C., Engrand, C., Nagashima, K., Brearley, A. J., 2019. Mineralogy and
- oxygen isotope systematics of magnetite grains and a magnetite-dolomite assemblage in
- 532 hydrated fine-grained Antarctic micrometeorites. Meteorit. Planet. Sci. 54, 1973-1989.
- Dobrică, E., Nuth, J.A., Brearley, A. J., 2022. Fayalite formation through hydrothermal
- experiments: Insights into early fluid-assisted aqueous alteration processes on asteroids.
- 535 Meteorit. Planet. Sci. 57, 381-391.
- Doyle, P. M., Jogo, K., Nagashima, K., Krot, A. N., Wakita, S., Ciesla, F. J., Hutcheon, I. D.,
- 537 2015. Early aqueous activity on the ordinary and carbonaceous chondrite parent bodies
- recorded by fayalite. Nat. Comm. 6, 7444.
- Endreß, M., Bischoff, A., 1996. Carbonates in CI chondrites: clues to parent body evolution.
- 540 Geochim. Cosmochim. Acta 60, 489–507.
- Gránásy, L., Pusztai, T., Tegze, G., Warren, J. A., Douglas, J. F., 2005. Growth and form of
- 542 spherulites. Phys. Rev. E 72, 011605.
- Genge, M. J., Grady, M. M., Hutchison, R., 1997. The textures and compositions of fine-grained
- Antarctic micrometeorites: Implications for comparisons with meteorites. Geochim.
- 545 Cosmochim. Acta 61, 5149-5162.
- Grassmann, O., Löbmann, P., 2004. Biomimetic nucleation and growth of CaCO₃ in hydrogels
- incorporating carboxylate groups. Biomat. 25, 277-282.
- Hicks, L. J., MacArthur, J. L., Bridges, J. C., Price, M. C., Wickham-Eade, J. E., Burchell, M.
- J., Hansford, G. M., Butterworth, A. L., Gurman, S. J., Baker, S. H., 2017. Magnetite in
- comet Wild 2: Evidence for parent body aqueous alteration. Meteorit. Planet. Sci. 52, 2075-
- 551 2096.

- Hua, X., Buseck, P. R., 1998. Fayalite in the Kaba and Mokoia carbonaceous chondrites.
- 553 Geochim. Cosmochim. Acta 59, 563-578.
- Ito, M., Tomioka, N., Uesugi, M. et al., 2022. A pristine record of outer Solar System materials
- from asteroid Ryugu's returned sample. Nat. Astron. 6, 1163–1171, doi.org/10.1038/s41550-
- 556 022-01745-5.
- Izawa, M. R. M., Cloutis, E. A., Rhind, T., Mertzman, S. A., Applin, D. M., Stromberg, J. M.,
- Sherman, D. M., 2019. Spectral reflectance properties of magnetites: Implications for remote
- sensing. Icarus 319, 525-539.
- Jedwab, J., 1965. Structures framboidal dans la météorite d'Orgueil. Acad. Sci. Paris 261, 923-
- 561 2925.
- Jedwab, J., 1967. La magnétite en plaquettes des météorites carbonées d'Alais, Ivuna et Orgueil.
- 563 Earth Planet. Sci. Lett. 2, 440-444.
- Jilly-Rehak, C. E., Huss, G. R., Nagashima, K., Schrader, D. L., 2018. Low-temperature
- aqueous alteration on the CR chondrite parent body: Implications from in situ oxygen-isotope
- analyses. Geochim. Cosmochim. Acta 222, 230-252.
- Joy, K. H., Visscher, C., Zolensky, M. E., Mikouchi, T., Hagiya, K., Ohsumi, K., Kring, D. A.,
- 568 2015. Identification of magnetite in lunar regolith breccia 60016: Evidence for oxidized
- conditions at the lunar surface. Meteorit. Planet. Sci. 50, 1157-1172.
- Keller, L. P., 1998. A TEM study of iron-nickel carbides in the matrix of the Semarkona
- unequilibrated ordinary chondrite. Meteorit. & Planet. Sci. 33, 913-919.
- Kerridge, J. F., Mackay, A. L., Boynton, W. V., 1979. Magnetite in CI carbonaceous meteorites:
- Origin by aqueous activity on a planetesimal surface. Science 205, 395-397.
- Kimura, Y., Sato, T., Nakamura, N., Nozawa, J., Nakamura, T., Tsukamoto, K., Yamamoto,
- 575 K., 2013. Vortex magnetic structure in framboidal magnetite reveals existence of water
- droplets in an ancient asteroid. Nat. Comm. 4, 1-8.
- Klein, C., 2005. Some Precambrian banded iron-formations (BIFs) from around the world:
- Their age, geologic setting, mineralogy, metamorphism, geochemistry, and origin. Amer.
- 579 Min. 90, 1473-1499.
- 580 Krot, A. N., Zolensky, M. E., Wasson, J. T., Scott, E. R. D., Keil, K., Ohsumi, K., 1997.
- Carbide-magnetite assemblages in type-3 ordinary chondrites. Geochim. Cosmochim. Acta
- 582 61, 219-237.

- Lefaucheux, F., Robert, M. C., Manghi, E., 1982. A comparison between gel grown and solution
- grown crystals Case of ADP and KDP. J. of Crystal Growth, 56, 141-150.
- Le Guillou, C., Brearley, A. J. 2014. Relationships between organics, water and early stages of
- aqueous alteration in the pristine CR3.0 chondrite MET 00426. Geochim. Cosmochim. Acta
- 587 131, 344–367.
- Le Guillou, C., Changela, H. G., Brearley, A. J. 2015. Widespread oxidized and hydrated
- amorphous silicates in CR chondrites matrices: Implications for alteration conditions and H₂
- degassing of asteroids. Earth Planet. Sci. Lett. 420, 162–173.
- Lofgren, G., 1974. An experimental study of plagioclase crystal morphology: Isothermal
- 592 crystallization. Americ. J. Sci. 274, 243-273.
- Magill, J. H., 2001. Spherulites: A personal perspective. J. of Mater. Sci. 36, 3143-3164.
- Matsumoto, T., Noguchi, T., Miyake, A., Igami, Y., Haruta, M., Seto, Y., 2022. Re-distribution
- of volatiles on airless surface of the C-type carbonaceous asteroid Ryugu. Nat. Astro. In
- review.
- McAlister, J. A., Kettler, R. M., 2008. Metastable equilibria among dicarboxylic acids and the
- oxidation state during aqueous alteration on the CM2 chondrite parent body. Geochim.
- 599 Cosmochim. Acta 72, 233-241.
- McCollom, T. M., Robbins, M., Moskowitz, B., Berquó, T. S., Jöns, N., Hynek, B. M., 2013.
- Experimental study of acid-sulfate alteration of basalt and implications for sulfate deposits
- on Mars. J. of Geophy. Res. 118, 577-614.
- McKay, C. P., Friedmann, E. I., Frankel, R. B., Bazylinski, D. S., 2003. Magnetotactic bacteria
- on Earth and on Mars. Astrobiology, vol. 3, 263-270.
- McSween, H. Y., Treiman, A. H., 1998. Martian meteorites. In Planetary materials, edited by
- Papike J. J. Reviews in Mineralogy, vol. 36. Washington, D.C.: Mineralogical Society of
- 607 America. pp. 6.1-6.53.
- Mittlefehldt, D. W., McCoy, T. J., Goodrich, C. A., Kracher, A., 1998. Non-chondritic
- meteorites from asteroidal bodies. In Planetary materials, edited by Papike J. J., Reviews in
- Mineralogy, vol. 36, Washington, D.C.: Mineralogical Society of America. pp. 4.1-4.195.
- Nakamura, E., Kobayashi, K., Tanaka, R., Kunihiro, T., Kitagawa, H., Potiszil, C. et al., 2022.
- On the origin and evolution of the asteroid Ryugu: A comprehensive geochemical
- 613 perspective. Proc. Jpn. Acad., Ser. B 98, 227-282.

- Nakamura, T., Matsumoto, M., Amano, K., Enokido, Y., Zolensky, M. E., et al., 2022.
- Formation and evolution of carbonaceous asteroid Ryugu: Direct evidence from returned
- samples. Science, doi 10.1126/science.abn8671.
- Noguchi, T., Nakamura, T., Nozaki, W., 2002. Mineralogy of phyllosilicate-rich
- micrometeorites and comparison with Tagish Lake and Sayama meteorites. Earth Planet. Sci.
- 619 Lett. 202, 229-246.
- Noguchi, T., Yabuta, H., Itoh, S., Sakamoto, N., Mitsunari, T., Okubo, A., Okazaki, R.,
- Nakamura, T., Tachibana, S., Terada, K., Ebihara, M., Imae, N., Kimura, M., Nagahara, H.,
- 622 2017. Variation of mineralogy and organic material during the early stages of aqueous
- activity recorded in Antarctic micrometeorites. Geochim. Cosmochim. Acta 208, 119-144.
- Noguchi, T., Matsumoto, T., Miyake, A., Igami, Y., Haruta, M., et al. 2022. A dehydrated
- space weathered skin cloaks the hydrated interior of Ryugu. Nat. Astro. in press.
- Nozawa, J., Tsukamoto, K., van Enckevort, W., Nakamura, T., Kimura, Y., Miura, H., Satoh,
- H., Nagashima, K., Konoto, M., 2011. Magnetite 3D colloidal crystals formed in the early
- solar system 4.6 billion years ago. J. of the Amer. Chem. Soc. 133, 8782-8785.
- Okazaki, R., Miura, Y. N., Takano, Y., Sawada, H., Sakamoto, K., Yada, T., et al. 2022. First
- asteroid gas sample delivered by the Hayabusa2 mission: A treasure box from Ryugu.
- 631 Science DOI: 10.1126/science.abo0431.
- Prus, M., Li, C., Kędra-Królik, K., Piasecki, W., Lament, K., Begović, T., Zarzycki, P., 2021.
- Unseeded, spontaneous nucleation of spherulitic magnesium calcite. Journal of Colloid and
- 634 Interface Science 593, 359-369.
- Ramdohr, P., 1963. Opaque minerals in stony meteorites. J. Geophys. Res. 68, 2011-2036.
- Rizzato, S., Moret, M., Merlin, M., Albinati, A., Beghi, F., 2016. Crystal growth in gelled
- solution: Applications to coordination polymers. CrystEngComm, 18, 2455.
- Roedder, E., 1984. Fluid Inclusions. Reviews in Mineralogy, Vol. 12, Mineralogical Society of
- 639 America, 644 p.
- Rosenberg, N. D., Browning, L., Bourcier, W. L., 2001. Modeling of aqueous alteration of CM
- carbonaceous chondrites. Meteorit. Planet. Sci. 36, 239-244.
- Rowe, M. W., Clayton, R. N., Mayeda, T. K., 1994. Oxygen isotopes in separated components
- of CI and CM meteorites. Geochim. Cosmochim. Acta 58, 5341-5347.

- Sato, M., Kimura, Y., Tanaka, S., Hatakeyama, T., Sugita, S., Nakamura, T., Tachibana, S.,
- Yurimoto, H., Noguchi, T., Okazaki, R., Yabuta, H., Naraoka, H., Sakamoto, K., Yada, T.,
- Nishimura, M., Nakato, A., Miyazaki, A., Yogata, K., Abe, M., Okada, T., Usui,
- T., Yoshikawa, M., Saiki, T., Terui, F., Nakazawa, S., Watanabe, S., Tsuda, Y., 2022. Rock
- magnetic characterization of returned samples from asteroid (162173) Ryugu: implications
- for paleomagnetic interpretation and paleointensity estimation. JGR Planets, in press.
- Schramm, L. S., Brownlee, D. E., Wheelock, M. M., 1989. Major element composition of
- stratospheric micrometeorites. Meteoritics 24, 99.
- Schulte, M., Shock, E., 2004. Coupled organic synthesis and mineral alteration on meteorite
- parent bodies. Meteorit. Planet. Sci. 39, 1577-1590.
- Shtukenberg, A. G., Punin, O. Y., Gunn, E., Kahr, B., 2012. Spherulites. Chem. Rev., 112,
- 655 1805-1838.
- 656 Siódmiak, J., Gadomski, A., 2022. Spherulites: How do they emerge at an onset of
- nonequilibrium kinetic-thermodynamic and structural singularity addressing conditions?
- 658 Entropy, 24, 663.
- Smith, R. K., Tremallo, R. L., Lofgren, G. E., 2001. Growth of megaspherulites in a rhyolitic
- of the vitrophyre. Amer. Min. 86, 589-600.
- Stodolna, J., Jacob, D., Leroux, H., 2012. Mineralogy and petrology of Stardust particles
- encased in the bulb of track 80: TEM investigation of the Wild 2 fine-grained material.
- Geochim. Cosmochim. Acta 87, 35-50.
- Tachibana, S., Sawada, H., Okazaki, R., Takano, Y., Sakamoto, K., et al. 2022. Pebbles and
- sand on asteroid (162173) Ryugu: In situ observation and particles returned to Earth. Science
- DOI: 10.1126/science.abj8624.
- Tall, D., Wagner, A., 2022. The gel growth technique—A neglected yet effective tool to prepare
- crystals of oxysalts and supergene minerals. Minerals 12, 645.
- Tsuchiyama, A., Miyake, A., Okuzumi, S., Kitayama, A., Kawano, J., Uesugi, K., Takeuchi,
- A., Nakano, T., Zolensky, M., 2021. Discovery of primitive CO₂-bearing fluid in an
- aqueously altered carbonaceous chondrite. Sci. Adv. DOI: 10.1126/sciadv.abg9707.
- Tsuchiyama, A., Matsumoto, M., J. Matsuno, Nakamura, T., Noguchi, T., Yasutake, M.,
- Uesugi, K., Takeuchi, A., Miyake, A., Okumura, S., Enju, S., Mitsukawa, I., Fujioka, Y.,
- Sun, M., Takigawa, A., Enokido, Y., Kawamoto, T., Morita, T., Kikuiri, M., Amano, K.,

- Kagawa, E., Matsumoto, T., Nakano, N., Rubino, S., Nakano, T., Yurimoto, H., Okazaki, R.,
- Yabuta, H., Naraoka, H., Sakamoto, K., Tachibana, S., Watanabe, S., Tsuda, Y., the
- Hayabusa2-initial-analysis Stone and Sand teams, 2022. 3D morphologies of magnetite,
- sulfides, carbonates and phosphates in Ryugu samples and their crystallization sequence
- during aqueous alteration. In: 85th Annual Meeting of the Meteoritical Society, abstr. #6221.
- Velásquez-González, O., Campos-Escamilla, C., Flores-Ibarra, A., Esturau-Escofet, N.,
- Arreguin-Espinosa, R., Stojanoff, V., Cuéllar-Cruz, M., Moreno, A., 2019. Crystal growth
- in gels from the mechanisms of crystal growth to control of polymorphism: New trends on
- theoretical and experimental aspects. Crystals, 9, 443.
- Wark, S. E., Hsia, C.-H., Hee Son, D., 2008. Effects of ion solvation and volume change of
- reaction on the equilibrium and morphology in cation-exchange reaction of nanocrystals. J.
- 686 Am. Chem. Soc. 130, 29.
- Xu, Y., Hao, H., Liu, P., Wang, Q., Sun, Y., Zhang, G., 2014. Facile synthesis, shape evolution
- and magnetic properties of polyhedral 50-facet Fe₃O₄ nanocrystals partially enclosed by
- 689 {311} high-index planes. Cryst. Eng. Comm. 16, 10451.
- Yada, T., Abe, M., Okada, T., Nakato, A., Yogata, K., Miyazaki, A., et al., 2022. Preliminary
- analysis of the Hayabusa2 samples returned from C-type asteroid Ryugu. Nat. Astron. 6,
- 692 214-220.
- Yokoyama, T., Nagashima, K., Nakai, I., Young, E.D., Abe, Y., et al., 2022. Samples returned
- from the asteroid Ryugu are similar to lyuna-type carbonaceous meteorites. Science
- 695 10.1126/science.abn7850.
- Zheng, Y.-F., 2011. On the theoretical calculations of oxygen isotope fractionation factors for
- carbonate-water systems. Geochem. J. 45, 341-354.
- Zheng, W., Hauwiller, M.R., Liang, W.-I., Ophus, C., Ercius, P., Chan, E.M., Chu, Y.-H., Asta,
- M., Du, X., Alivisatos, A.P., Zheng, H., 2019. Real time imaging of two-dimensional iron
- oxide spherulite nanostructure formation. Nano Res., 12, 2889-2893.
- Zhu, Y., Ophus, C., Toloczko, M. B., Edwards, D., 2018. Diffraction contrast scanning
- transmission electron microscopy A bend-contour-free way to image dislocations, voids
- and precipitates. Microsc. Microanal. 24, #1472, doi:10.1017/S1431927618007845.
- Zolensky, M. E., Bourcier, W. L., Gooding, J. L., 1989. Aqueous alteration on the hydrous
- asteroids: Results of EQ3/6 computer simulations. Icarus 78, 411-425.

- Zolensky, M. E., Bodnar, R. J., Gibson, E. K., Gounelle, M., Nyquist, L. E., Reese, Y., Shih,
- 707 C.-Y., Wiesmann, H., 1999 Asteroidal water within fluid inclusion-bearing halite in an H5
- 708 chondrite. Science 285, 1377-1379.
- Zolensky, M. E., Krot, A. N., Benedix, G., 2008. Record of low-temperature alteration in
- asteroids. Rev. in Min. and Geochem. 68, 429-462.
- Zolensky, M. E., Bodnar, R. J., Yurimoto, H., Itoh, S., Fries, M., Steele, A., Chan, Q. H.-S.,
- Tsuchiyama, A., Kebukawa, Y., Ito, M., 2017. The search for and analysis of direct samples
- of early Solar System aqueous fluids. Phil. Trans. R. Soc. A 375, 20150386.
- Zolensky, M. E., Dolocan, A., Bodnar, R., Gearba, I., Martinez, J., Han, J., Nakamura, T.,
- Tsuchiyama, A., Matsuno, J., Sun, M., Matsumoto, M., Fujioka, Y., Enokido, Y., Uesugi,
- K., Takeuchi, A., et al., 2022. Direct measurement of the composition of aqueous fluids from
- 717 the parent body of asteroid 162173 Ryugu. Lunar Planet. Sci. Conf. 53. abstr. #1451.
- Zolotov, M. Y., 2012. Aqueous fluid composition in CI chondritic materials: Chemical
- equilibrium assessments in closed systems. Icarus 220, 713-729.

Figure 1. Backscattered (a-e) and secondary (f) electron images of magnetite with different morphologies (a – framboidal and magnetite spherules; b – plaquettes; and c – spherulitic and single dodecahedron) embedded in the fine-grained materials returned by the Hayabusa2 spacecraft collected during the second touchdown (chamber C). Figure 1d-f shows one of the spherulitic magnetite (~13 μm in diameter) analyzed in this study (sample C0105-039024). One focused ion beam (FIB) section (e - white dashed line) was prepared for transmission electron microscopy (TEM) study in this sample. Minerals identified: mt – magnetite, phy – phyllosilicates, and S – sulfide.

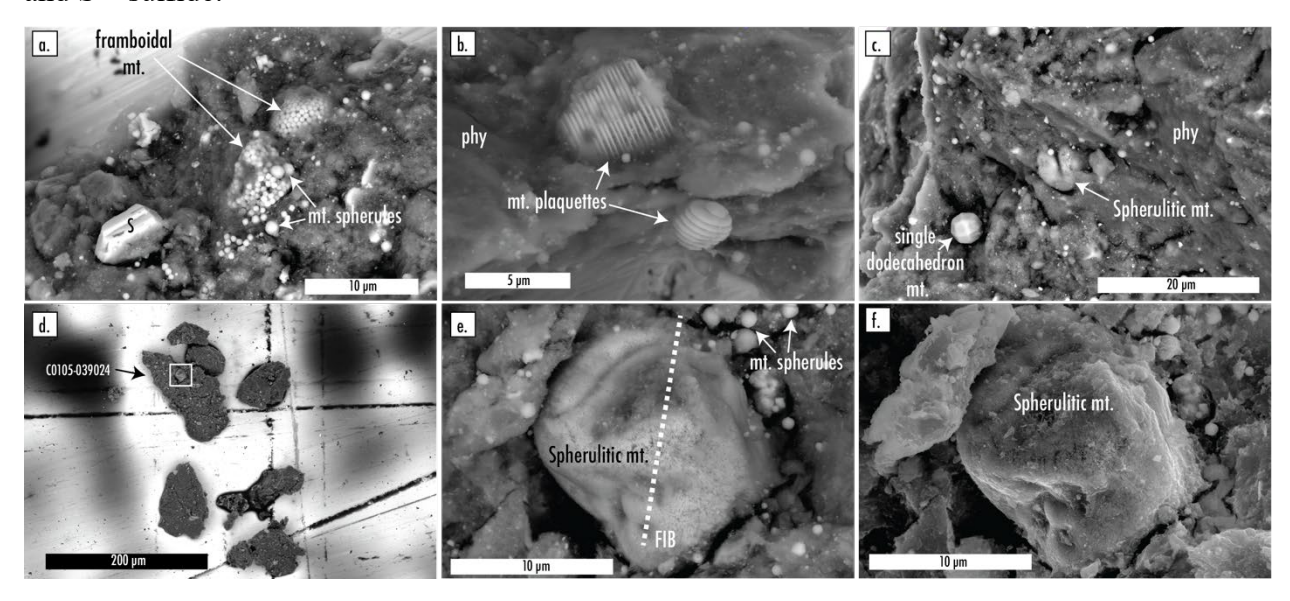


Figure 2. Bright-field scanning transmission electron microscopy (STEM) images of the mineral phases identified in the one of the Hayabusa2 particles, focused ion beam section (FIB) A0104-00200201, collected during the first touchdown (chambers A). Both framboidal and spherulitic magnetite (mt, Fig. 2a) are identified to be associated with euhedral sulfides (S), an organic nanoglobule embedded in a coarse-grained matrix of phyllosilicates (phy.). The spherulitic magnetite is composed of radial fibers (Fig. 2b). Euhedral (Fig. 2c, black arrows) to anhedral pores are homogeneously distributed in this magnetite. Additionally, euhedral laths (Fig. 2d) were identified at the surface of the spherulitic magnetite grain. The platinum (Pt) strap is at the top of the FIB section. Two diffraction patterns were indexed as [111] for the framboidal magnetite (Fig. 2a) and [011] zone axis (directions are also shown) of spherulitic magnetite (Fig. 2d).

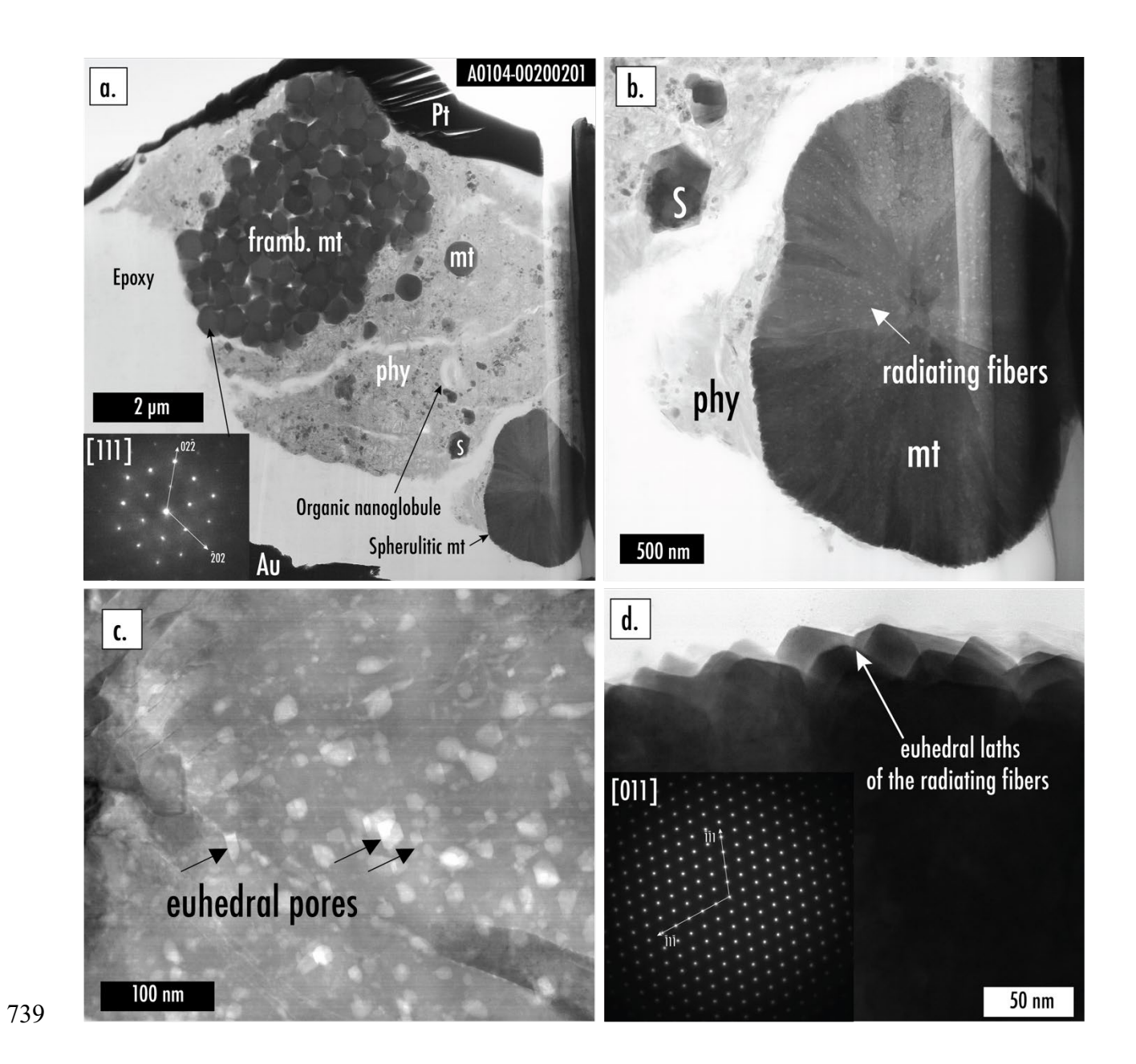


Figure 3. Bright- (a-b, e-f) and dark-field STEM (g-h) images and diffraction patterns (c-d) of the spherulitic magnetite analyzed from chamber C (C0105-039024). STEM micrographs (b, e-f) were taken using a beam convergence that provides better contrast. These diffraction contrast STEM images (Fig. 3b, and e-f) show the occurrence of pervasive dislocations (Fig. 3f) in the magnetite fibers. The TEM data show the texture of the radiating fibers and the pervasive distribution of euhedral to subhedral pores. Most euhedral pores are elongated parallel to the radiating fibers (Fig. 3h). The fibers' orientation is marked with a black arrow with a dashed line, and the fibers' boundaries with a withe dashed line (Fig. 3h). A spherical pore (~130 nm in diameter) located off-center was identified in this spherulitic magnetite (Fig. 3b and 3g). Two diffraction patterns (Figs. 3c-d) were indexed as [136] zone axis (directions are also shown) of magnetite showing the same crystallographic orientation between the magnetite fibers, indicating that this spherulitic magnetite is a single crystal; however, some domains may have slight misorientations. The locations of the diffraction patterns are indicated by the numbered white circles (Fig. 3b). An organic nanoglobule was identified in the phyllosilicates in contact with the spherulitic magnetite (Fig. 3e). Minerals identified: mt – magnetite, phy – phyllosilicates, and S – sulfide.

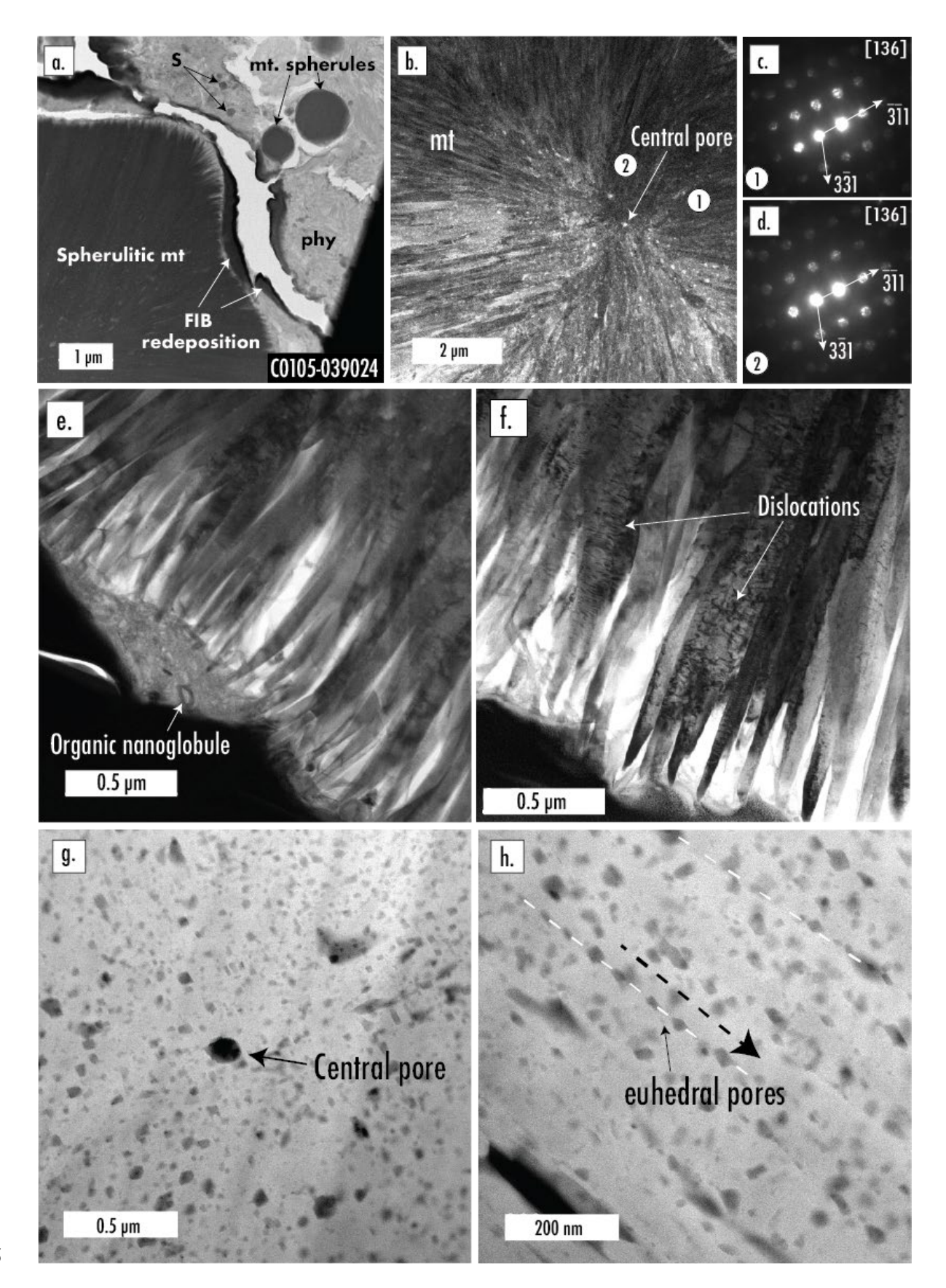


Figure 4. Dark-field STEM images of magnetite spherules identified in sample A104-01300103 showing the presence of anhedral to subhedral pores with a diameter of \sim 10 nm (see arrows in Fig. 4c); however, these spherules are texturally featureless compared with the spherulites. The magnetite spherules (Fig. 4a) have variable sizes from 0.6 μ m to 1.2 μ m in diameter.

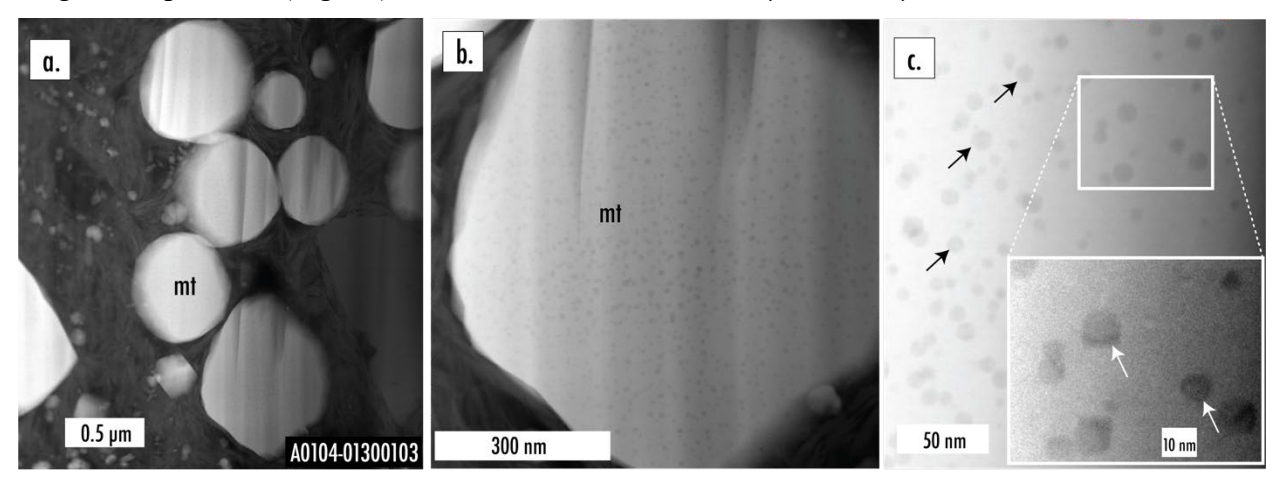


Figure 5. a-b) Bright-field (BF) transmission electron microscope (TEM) images of an irregular shaped spherulitic magnetite analyzed from chamber A (A0104-00100401) consisting of crystal domains (~100 nm in diameter), some of which show 3-fold periodicity along one of the <111> directions. The neighboring crystals in the aggregate have epitaxial relationships. c-h) Nanobeam diffraction patterns of the irregular shaped spherulitic magnetite obtained from white rectangle shown in Figure 5b. c) Virtual BF image reconstructed from the nanobeam diffraction (NBD) dataset. d-f) Diffraction patterns extracted from the regions shown in Figure 5c. g) Virtual dark-field image reconstructed from the virtual detectors shown in Figure 5h. Three images are superimposed as pseudocolor in (g) and (h); white corresponds to basic reflections of magnetite, red corresponds to superlattice reflections indicating 3-fold periodicity along [111]*, and green corresponds to superlattice reflections indicating 3-fold periodicity along [111]*.

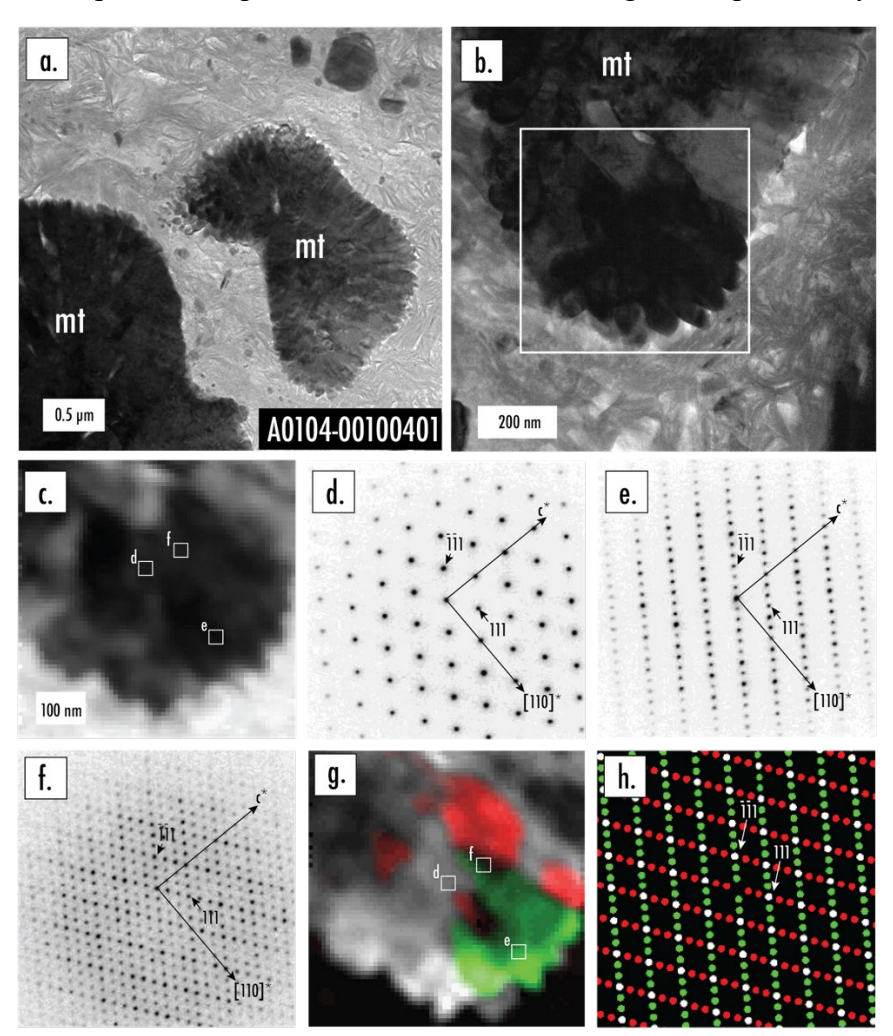


Figure 6. Dark-field (Fig 6a-b, 6d) images and energy-dispersive X-ray spectroscopy (EDS) maps (Fig. 6c and 6e) made by scanning transmission electron microscopy (STEM) showing the spherulitic magnetite from sample A104-01300103, which contain amorphous materials in several pores (Fig. a-c) and at the edges of the acicular fibers (Fig. 6d-e). The compositions of these amorphous materials are shown in Table 1. The white rectangle (Fig. 6a) shows the region where the EDS map of Fe and Si was made. The composite EDS map (Fig. 6c) shows the distribution of amorphous Si-rich materials inside the pores. Additionally, we show the composite EDS map (Fig. 6e) of the Fe, Si, and Mg at the edges of the acicular fibers of magnetite. The compositions of the two regions (A and B) are shown in Table 1.

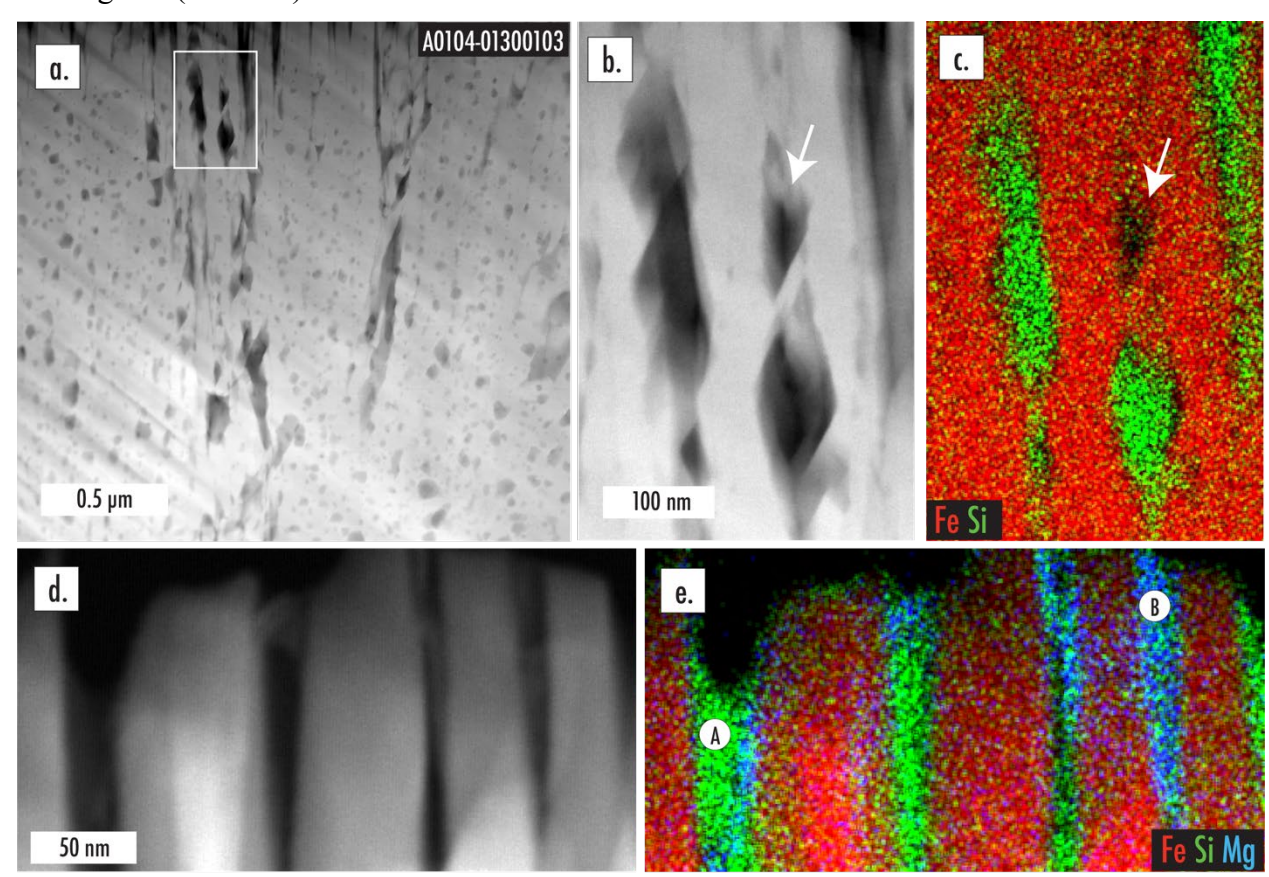


Table 1. Concentration of major and minor elements (in atom%) determined by analytical scanning transmission electron microscopy (STEM) energy dispersive X-ray spectroscopy (EDS) of the amorphous materials (am. mat.) identified inside the pores (Fig. 6c) and at the edges of the acicular fibers (Fig. 6e, region A – Si-rich and region B – Si- and Mg-rich amorphous materials) and of the spherulitic magnetite from sample A104-01300103.

| | Pores | | Si-rich am. mat.* Si-, Mg-rich am. m | | ıt.** | |
|---------|---------|------|--------------------------------------|-----|---------|------|
| Locatio | | | | | | |
| n | Fig. 6c | | Fig. 6e | | Fig. 6e | |
| | | | | S.D | | |
| N | 7 | S.D. | 7 | • | 4 | S.D. |
| Si | 6.6 | 1.5 | 25.4 | 4.7 | 10.9 | 1.2 |
| Al | 0.1 | 0.1 | 0.2 | 0.2 | 0.2 | 0.4 |
| Ti | 0.1 | 0.0 | - | - | 0.1 | 0.0 |
| Cr | 0.1 | 0.1 | - | - | - | - |
| Fe | 34.7 | 2.5 | 6.2 | 3.2 | 14.9 | 4.3 |
| Mg | - | - | 1.4 | 1.7 | 8.8 | 1.9 |
| Ca | | | 0.1 | 0.1 | - | - |
| Na | | | 0.1 | 0.1 | 1.9 | 1.7 |
| K | - | - | - | - | 0.1 | 0.1 |
| S | | | 0.1 | 0.1 | 0.2 | 0.3 |
| Ni | - | - | - | - | 0.1 | 0.1 |
| O | 58.4 | 1.7 | 66.4 | 1.6 | 62.7 | 0.6 |
| Total | 100.0 | | 100.0 | | 100.0 | |

⁷⁸⁸ S. D. – standard deviation

783

784

785

786

^{789 *}Composition of region A from Figure 6e.

^{790 **}Composition of region B from Figure 6e.